LETTER

doi:10.1038/nature10454

Metabolic priming by a secreted fungal effector

Armin Djamei[1]*, Kerstin Schipper[1,2]*†, Franziska Rabe[1], Anupama Ghosh[1], Volker Vincon[1], Jörg Kahnt[1], Sonia Osorio[3], Takayuki Tohge[3], Alisdair R. Fernie[3], Ivo Feussner[4], Kirstin Feussner[5], Peter Meinicke[5], York-Dieter Stierhof[6], Heinz Schwarz[7], Boris Macek[8]†, Matthias Mann[8] & Regine Kahmann[1]

Maize smut caused by the fungus *Ustilago maydis* is a widespread disease characterized by the development of large plant tumours. *U. maydis* is a biotrophic pathogen that requires living plant tissue for its development and establishes an intimate interaction zone between fungal hyphae and the plant plasma membrane. *U. maydis* actively suppresses plant defence responses by secreted protein effectors[1,2]. Its effector repertoire comprises at least 386 genes mostly encoding proteins of unknown function[1,3,4] and expressed exclusively during the biotrophic stage[3]. The *U. maydis* secretome also contains about 150 proteins with probable roles in fungal nutrition, fungal cell wall modification and host penetration as well as proteins unlikely to act in the fungal-host interface[4] like a chorismate mutase. Chorismate mutases are key enzymes of the shikimate pathway and catalyse the conversion of chorismate to prephenate, the precursor for tyrosine and phenylalanine synthesis. Root-knot nematodes inject a secreted chorismate mutase into plant cells likely to affect development[5,6]. Here we show that the chorismate mutase Cmu1 secreted by *U. maydis* is a virulence factor. The enzyme is taken up by plant cells, can spread to neighbouring cells and changes the metabolic status of these cells through metabolic priming. Secreted chorismate mutases are found in many plant-associated microbes and might serve as general tools for host manipulation.

The *U. maydis* genome (http://mips.helmholtz-muenchen.de/genre/proj/ustilago) contains genes for both a cytosolic chorismate mutase, designated *aro7* (*um04220*), and a putatively secreted chorismate mutase, *cmu1* (*um05731*). Cmu1 belongs to the AroQ class of eukaryotic chorismate mutases (Interpro: IPR008238) that have an all-α-helical secondary structure (Supplementary Fig. 1)[7,8]. To verify that Cmu1 is a dedicated chorismate mutase, we demonstrated that it complemented a *Saccharomyces cerevisiae aro7* mutant (Fig. 1a) and that heterologously expressed protein had chorismate mutase activity which was not feedback inhibited by aromatic amino acids (Supplementary Fig. 2). Allosteric regulation is a characteristic feature of plastidic chorismate mutases as well as of cytoplasmic fungal chorismate mutases[9,10], whereas cytosolic plant chorismate mutases lack this feature[11]. Attempts to generate a *cmu1* mutant that displayed allosteric regulation based on features of *S. cerevisiae* Aro7p were unsuccessful (Supplementary Fig. 3). Western blot analysis detected Cmu1–haemagglutinin (HA) in *U. maydis* culture supernatants when the respective fusion gene was expressed under a constitutive promoter in hyphal cells (Supplementary Fig. 4). The secretion of Cmu1 during plant colonization was independently demonstrated by proteome analysis of apoplastic fluids isolated after infection of maize with a mixture of compatible *U. maydis* strains. Compared with known secreted effector proteins like Mig2 (ref. 12), higher numbers of Cmu1 peptides were identified at all time points analysed (Supplementary Information, Table 1).

Like many other *U. maydis* effectors with a virulence function[1,3,13], *cmu1* is specifically upregulated during biotrophic development (Supplementary Fig. 5) and is one of the most highly expressed fungal genes during plant colonization[14]. To determine a possible contribution to virulence *cmu1* was deleted in the solopathogenic strains SG200 (ref. 3) and CL13. CL13 is the progenitor strain of SG200 that shows attenuated virulence[15] (see Supplementary Fig. 6a for disease

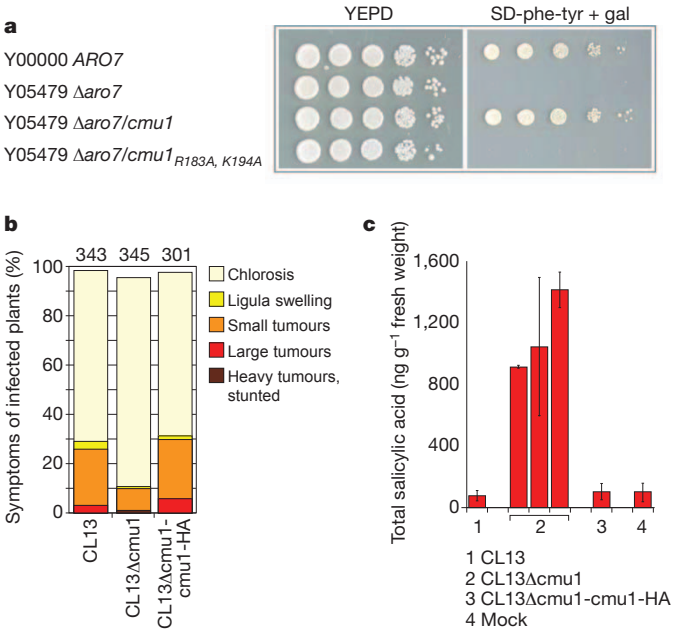

Figure 1 | Cmu1 has chorismate mutase activity, affects virulence and salicylic acid levels. a, *U. maydis cmu1* complements the *aro7* deletion in *S. cerevisiae*. Growth of the *S. cerevisiae aro7* deletion mutant Y05479 on medium lacking tyrosine and phenylalanine (SD-phe-tyr) is restored by introduction of *U. maydis cmu1*; whereas $cmu1_{R183A,K193A}$ does not complement. Expression of *cmu1* genes was driven by the *GAL1* promoter. *S. cerevisiae* Y00000 (native *ARO7* gene) was used as positive control. YEPD, rich medium; gal, galactose. **b**, Deletion of *cmu1* negatively affects virulence of *U. maydis* strain CL13. Disease symptoms (as depicted in Supplementary Fig. 6a) on maize plants were scored[3] 12 days after infection with the indicated strains. Mean values of seven independent infections are shown with the total number of infected plants indicated above each column. Compared with CL13 and CL13Δcmu1-cmu1–HA, CL13Δcmu1 showed significantly reduced tumour formation (*t*-test, $P = 0.037$). **c**, Total amounts of salicylic acid were determined in plant leaves infected with the indicated *U. maydis* strains listed below 8 days after infection. For the infections with CL13Δcmu1, three independent strains were used. Mean values of three independent experiments are shown. Error bars, s.d.

[1]Max Planck Institute for Terrestrial Microbiology, Karl-von-Frisch-Straße 10, D-35043 Marburg, Germany. [2]Zentrum Synthetische Mikrobiologie, Philipps-Universität Marburg, D-35032 Marburg, Germany. [3]Max Planck Institute of Molecular Plant Physiology, Wissenschaftspark Golm, Am Mühlenberg 1, D-14476 Potsdam-Golm, Germany. [4]Georg-August-University, Albrecht-von-Haller Institute, Justus-von-Liebig Weg 11, D-37077 Göttingen, Germany. [5]Georg-August-University, Institute for Microbiology and Genetics, Grisebachstraße 8, D-37077 Göttingen, Germany. [6]Center for Plant Molecular Biology, University of Tübingen, Auf der Morgenstelle 5, D-72076 Tübingen, Germany. [7]Max Planck Institute for Developmental Biology, Spemannstraße 35, D-72076 Tübingen, Germany. [8]Max Planck Institute for Biochemistry, Am Klopferspitz 18, D-82152 Martinsried, Germany. †Present addresses: Heinrich-Heine-Universität, Abteilung Mikrobiologie, Gebäude 26.12, Ebene 01, Universitätsstrasse 1, D-40225 Düsseldorf, Germany (K.S.); Proteome Center Tuebingen, Auf der Morgenstelle 15, D-72076 Tübingen, Germany (B.M.).
*These authors contributed equally to this work.

symptoms of CL13) and hence facilitates the detection of modest differences in virulence[16]. Whereas SG200Δcmu1 strains showed little virulence attenuation (Supplementary Fig. 6b), the CL13Δcmu1 mutant displayed a reduction of about 50% in tumours, which could be complemented by introducing a single copy of *cmu1–HA* (Fig. 1b). This illustrates that Cmu1 is required for full virulence and demonstrates functionality of the HA-tagged protein.

To localize Cmu1 during biotrophic growth, plants were infected with SG200Δcmu1-cmu1–HA, which carries a *cmu1–HA* fusion gene inserted in single copy under control of its native promoter. Plants infected with SG200 or with SG200 P_{cmu1}GFP–HA expressing cytoplasmic green fluorescent protein (GFP) under the *cmu1* promoter served as negative controls. Freeze-substituted and resin-embedded sections of maize tissue harvested 3 days after infection with these strains were incubated with anti-HA antibodies and gold markers. Cmu1–HA could be detected inside the fungal hyphae, in the biotrophic interface as well as inside the plant cytoplasm but rarely in the plant cell wall (Fig. 2A and Supplementary Fig. 7). The distribution of gold particles was quantified (Fig. 2B). Gold labelling of plant tissue infected with the parental strain SG200 was negligible (Supplementary Fig. 8), whereas non-secreted GFP–HA was absent from the biotrophic interphase, showed strong accumulation in the fungal cytosol and weak background labelling in the plant cytosol (Supplementary Fig. 9 and Fig. 2B). Integrity of Cmu1–HA was demonstrated by western blot analysis after immunoprecipitation from infected plant tissue (Supplementary Fig. 10). To demonstrate Cmu1 localization independently, plants were infected with SG200Δcmu1-cmu1–mCherry–HA. Cmu1–mCherry–HA was detected in the biotrophic interface, and plasmolysis experiments showed that it freely diffused in the enlarged apoplast (Supplementary Fig. 11). However, fluorescence could not be detected inside plant cells. In addition, Cmu1–mCherry–HA was unable to complement the virulence phenotype of CL13Δcmu1 (Supplementary Fig. 12a) despite the fact that the fusion protein was enzymatically active as demonstrated by complementation of the *aro7* yeast mutant (Supplementary Fig. 13). $Cmu1_{22–290}$–HA lacking the secretion signal was unable to complement the virulence phenotype of CL13Δcmu1 (Supplementary Fig. 12b), demonstrating that secretion is prerequisite for function. In sum, these data suggest that Cmu1 needs to enter plants cells to exert its function and that Cmu1–mCherry–HA is unable to do so.

To elucidate the subcellular localization of Cmu1 in plant cells, a $Cmu1_{22–290}$–mCherry fusion protein lacking the signal peptide and active in complementing the yeast *aro7* mutant was transiently expressed in maize leaves (Supplementary Fig. 13). $Cmu1_{22–290}$–mCherry localized to the cytoplasm and the nucleus of transformed maize cells (Fig. 2C). Surprisingly, in some cases the $Cmu1_{22–290}$–mCherry signal was also visible in cells adjacent to the originally transformed cell (Fig. 2C, a). To rule out that the latter is caused by independent transformation events, $Cmu1_{22–290}$–yellow fluorescent protein (YFP) and $PIP_{426–593}$–mCherry encoding a fusion protein that localizes exclusively to the nucleus, were co-expressed (Supplementary Fig. 14). Cell-to-cell spreading of $Cmu1_{22–290}$–YFP was observed in some cases whereas $PIP_{426–593}$–mCherry always remained in the nucleus of the originally transformed cell (Supplementary Fig. 14). Occasionally guard cells were transformed, and in such cases spreading of $Cmu1_{22–290}$–YFP was never observed (Fig. 2C, c and Supplementary Fig. 14). Because guard cells lack plasmodesmata[17], the observed spreading of $Cmu1_{22–290}$ is likely to occur through plasmodesmata.

By yeast two-hybrid analysis we demonstrated that Cmu1 can dimerize (Supplementary Fig. 15a), a property characteristic for AroQ chorismate mutases[8]. In addition, Cmu1 could interact with the two maize chorismate mutases ZmCm1 (B6TU00) and ZmCm2 (B4FUP5) (Supplementary Fig. 15a). Despite low overall sequence conservation, known residues essential for chorismate mutase activity were conserved in all these enzymes (Supplementary Fig. 15b).

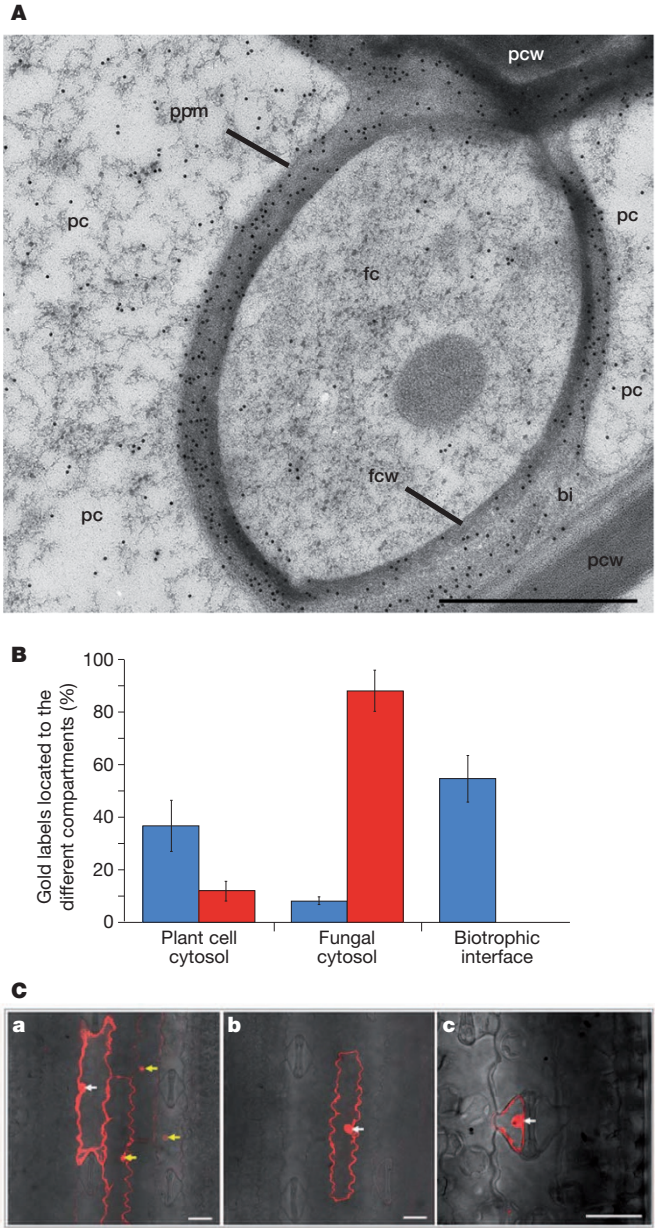

Figure 2 | Cmu1 is translocated to plant cells and spreads to neighbouring tissue. **A**, A maize section infected with *U. maydis* SG200Δcmu1-cmu1–HA was collected 3 days after infection, probed with mouse anti-HA antibodies and detected with anti-mouse antibodies conjugated to 12-nm gold particles (Methods). Electron micrographs visualize Cmu1–HA inside fungal hyphae, in the biotrophic interface and in the cytoplasm of infected maize cells. Leaves infected with SG200 and SG200 P_{cmu1}GFP–HA served as negative controls (Supplementary Figs 8 and 9). fc, fungal cytosol; fcw, fungal cell wall; bi, biotrophic interphase; pc, plant cytosol; pcw, plant cell wall; ppm, plant plasma membrane. Scale bars, 1 μm. **B**, Electron micrographs of immunogold-labelled sections were analysed for the spatial distribution of gold labels in SG200Δcmu1-cmu1–HA (blue) and SG200 P_{cmu1}GFP–HA (red) infected tissue 3 days after infection. The total number of gold labels in each electron micrograph was set to 100% (see Methods for details). Error bars, s.d. of gold particles counted in three independent cross-sections. **C**, Confocal Z-stacks visualize spreading of $Cmu1_{22–290}$–mCherry to neighbouring tissue after biolistic transformation of maize leaves. White arrows indicate the originally transformed maize cells that carry a gold particle in their nucleus (**a**–**c**). Spreading of the fluorescent signal was observed in some cases for Cmu1–mCherry (**a**) and not in others (**b**, **c**). Yellow arrows mark $Cmu1_{22–290}$–mCherry signals in nuclei of neighbouring cells (**a**). $Cmu1_{22–290}$–mCherry spreading was never detected in transformed guard cells (**c**). Scale bars, 40 μm.

ZmCm1 encodes a predicted plastidic isoform (Supplementary Fig. 16a) whereas ZmCm2 codes for a putative cytoplasmic enzyme (Supplementary Fig. 15b). Localization to the respective compartments was demonstrated by transient expression in maize leaves (Supplementary Fig. 16b, c). The observed compartmentalization mimics what has been described for the chorismate mutases of *Arabidopsis thaliana*[18]. Furthermore, as shown for the cytoplasmic isoform of chorismate mutase in *A. thaliana*[19], ZmCm2 displayed enzymatic activity but no allosteric regulation *in vitro* (Supplementary Fig. 15c).

To demonstrate that the interaction between Cmu1 and the cytosolic maize chorismate mutase ZmCm2 can have functional consequences, we attempted to show that Cmu1 could alter ZmCM2 activity *in vitro*. As this was unsuccessful (Supplementary Fig. 15d), we next generated a loss of function allele of *cmu1* based on catalytically inactive forms of *S. cerevisiae* Aro7p (Supplementary Fig. 1a)[20,21]. We reasoned that heterodimer formation between active and inactive monomers might interfere with chorismate mutase function. As expected, the $cmu1_{R183A,K194A}$ allele was unable to complement the *aro7* deletion in *S. cerevisiae* (Fig. 1a). Surprisingly, when $cmu1_{R183A,K194A}$ was introduced in single copy in either CL13Δcmu1 or SG200Δcmu1, virulence was completely abolished (Supplementary Fig. 17). When $cmu1_{R183A,K194A}$ was introduced in SG200 harbouring a functional *cmu1* allele, the mutated allele had a dominant effect that was copy number dependent (Supplementary Fig. 17). Confocal microscopy of infected leaf tissue revealed that the SG200Δcmu1–$cmu1_{R183A,K194A}$ strain could form appressoria (Supplementary Fig. 18a) but failed to colonize the plant (Supplementary Fig. 18b). In contrast to SG200 infections, plant cells infected with SG200Δcmu1-$cmu1_{R183A,K194A}$ were heavily stained by propidium iodide and displayed strong autofluorescence, probably because of the formation of phenolic compounds (Supplementary Fig. 18). This indicates that SG200Δcmu1-$cmu1_{R183A,K194A}$ elicits a strong plant defence response.

To exclude the possibility that the non-functional secreted chorismate mutase might interfere with the endogenous fungal shikimate pathway, we generated SG200Δcmu1 derivatives that express $cmu1_{R183A,K194A}$ under control of a strong constitutive promoter (SG200Δcmu1-$P_{otef}$$cmu1_{R183A,K194A}$–HA). Western blot analysis confirmed that the mutant protein was produced and secreted (Supplementary Fig. 19a). These strains did not show a growth phenotype on minimal media lacking aromatic amino acids, were morphologically indistinguishable from SG200 during growth in minimal media, and were unaltered in filamentous growth on charcoal media, a prerequisite for successful infection (Supplementary Fig. 19b–e). This illustrates that the secreted $Cmu1_{R183A,K194A}$–HA protein does not interfere with the activity of the cytoplasmic Aro7 protein in *U. maydis*. $Cmu1_{R183A,K194A}$-mCherry–HA accumulated around biotrophic hyphae like other secreted effectors[13] (Supplementary Fig. 20b) but was unable to cause a dominant negative virulence phenotype when expressed in SG200Δcmu1 (Supplementary Fig. 20a). This suggests that plant uptake of $Cmu1_{R183A,K194A}$–mCherry–HA is necessary for the dominant effect on virulence, presumably because activity of ZmCM2 is affected. To obtain evidence that $Cmu1_{R183A,K194A}$–HA can reduce ZmCm2 activity, we first showed that ZmCm2 was able to interact with $Cmu1_{R183A,K194A}$ and could complement the *aro7* mutation in *S. cerevisiae* (Supplementary Fig. 21). Next, *zmcm2* was co-expressed with *cmu1* or $cmu1_{R183A,K194A}$ in the yeast *aro7* mutant strain. Although the co-expression of *zmcm2* and *cmu1* had no detectable effect on growth, co-expression of *zmcm2* and $cmu1_{R183A,K194A}$ attenuated growth on plates lacking phenylalanine and tyrosine (Supplementary Fig. 21b). Therefore, the dominant negative effect on virulence elicited by the $cmu1_{R183A,K194A}$–*HA* allele is probably caused by interfering with the activity of cytosolic ZmCm2 through dimerization. This also implies that orphan cytosolic plant chorismate mutases might have an important regulatory function.

To obtain a comprehensive view on the metabolic changes in plants infected with CL13, CL13Δcmu1 and CL13Δcmu1-cmu1–HA, metabolome analyses were conducted 8 days after infection (Supplementary Figs 22 and 23 and Supplementary Table 2). Compared with mock-infected maize, plants infected with CL13 showed enhanced levels for phenylpropanoid and lignan biosynthesis products as well as for benzoxazinones, which derive from tryptophan (Supplementary Fig. 22 and Supplementary Table 3). For plants infected with CL13 and CL13Δcmu1, the most notable differences concerned the phenylpropanoid pathway (Supplementary Fig. 22). Substances such as coumaroyl- and caffeoylquinate and syringine as well as lignan (like the syringaresinol-glucosides) were less abundant in tissue infected with CL13Δcmu1 than in plants infected with either CL13 or the complemented strain CL13Δcmu1-cmu1–HA (Supplementary Fig. 22b and Supplementary Tables 2 and 3). In contrast, the amount of salicylic acid was at least ten times higher in plants infected with CL13Δcmu1 than those infected with the parental strain CL13 or CL13Δcmu1-cmu1–HA, respectively (Fig. 1c). The amounts of the tryptophan-derived benzoxazinones were not significantly different in CL13Δcmu1 and CL13 infections (Supplementary Fig. 22), indicating that the pathway from chorismate to tryptophan through anthranilate synthase is unaffected by Cmu1 activity. The underlying mechanism for this differential effect awaits further study. Our results support a situation in which Cmu1 channels chorismate into the phenylpropanoid pathway and prevents its flow into the salicylic acid biosynthesis branch.

To elucidate the biological significance of the elevated salicylic acid levels in CL13Δcmu1 infections, maize seedlings were treated locally with 4 mM salicylic acid before infection or co-infiltrated during the infection with CL13. This concentration was chosen on the basis of total salicylic acid levels determined in CL13Δcmu1-infected plants. Both treatments led to a reduction in virulence comparable to CL13Δcmu1 infections (Supplementary Fig. 24), which illustrates that salicylic acid enhances resistance of maize towards *U. maydis*. The data imply that the observed decrease in virulence for CL13Δcmu1 could be a direct consequence of its inability to interfere with pathogen-induced salicylic acid biosynthesis of the host plant.

Our findings provide new insights into a process that aids *U. maydis* during colonization of maize plants. It relies on the secretion of a chorismate mutase which enters plant cells by an unknown mechanism and redirects the metabolome in favour of the parasite.

We propose that the translocated fungal enzyme acts in conjunction with ZmCm2 in the plant cytosol by increasing the flow of chorismate from the plastid to the cytosol and in turn lowering the available substrate for salicylic acid biosynthesis in plastids (Fig. 3). However,

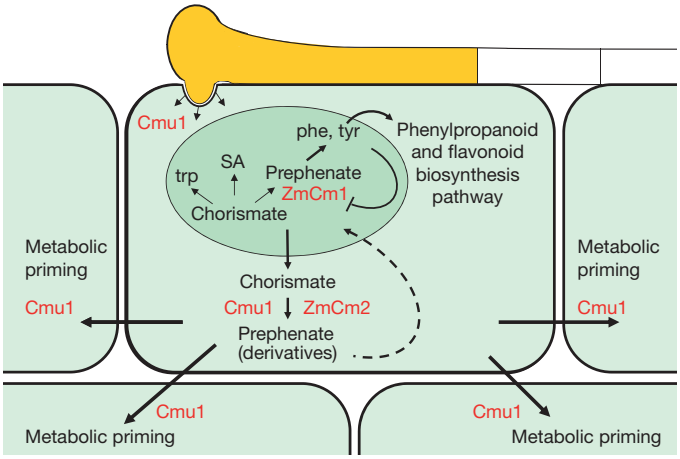

Figure 3 | Model of Cmu1-mediated metabolic priming in infected maize tissue. An infecting fungal hyphae is depicted in yellow. Maize cells are shown in mint green, the plastid is depicted in darker green. The dotted line indicates that prephenate or prephenate derivatives might be re-imported into the plastid or have regulatory capacity to feedback on plastidic synthesis of phenylalanine and tyrosine or derived phenolic compounds. SA, salicylic acid. For details, see text.

the introduction of a deregulated chorismate mutase into the host plant cytosol alone cannot explain all the metabolic changes observed in the *U. maydis* infected tissue (Supplementary Table 2 and Supplementary Fig. 18)[2,22]. Thus, in line with its modest effects on virulence, we consider Cmu1 to be one component of a cocktail of effectors shaping the host metabolome. In this context it might not be coincidence that *U. maydis* has genes for two potential salicylate hydroxylases. In addition, organ-specific functions as described for several other *U. maydis* effectors cannot be excluded[14].

The suppression of salicylic acid levels is likely to be particularly important for biotrophic pathogens and symbionts[23]. In line with this we found genes encoding secreted chorismate mutases in many genomes of eukaryotic biotrophic plant pathogens and symbionts and several hemibiotrophic plant pathogens but only rarely in necrotrophic plant pathogens and fungal saprophytes (Supplementary Table 4). Recent findings indicate that the secreted chorismate mutase in the fungus *Sclerotinia sclerotiorum* might also represent a virulence factor (M. Dickman, personal communication). Metabolic priming by secreted chorismate mutases might thus emerge as a common strategy for host manipulation.

METHODS SUMMARY

The Methods section provides detailed information about all experimental procedures, including the following: (1) tables with details on oligonucleotides, plasmids, *U. maydis* and *S. cerevisiae* strains used or generated in this study; (2) details on the cloning strategies; (3) description of *U. maydis* mutant generation and their subsequent analysis; (4) links to bioinformatic tools applied in this study; (5) details for conducting quantitative real-time PCR analyses; (6) description of the yeast complementation assays; (7) description of yeast protein interaction assays; (8) details for conducting chorismate mutase activity assays; (9) the method to demonstrate protein secretion in *U. maydis*; (10) details on the transient expression in *Zea mays*; (11) confocal and electron microscopy methods; (12) details for metabolome and hormone analyses; and (13) protocol for the isolation and mass spectrometric analysis of secreted proteins of apoplastic fluids.

Full Methods and any associated references are available in the online version of the paper at www.nature.com/nature.

Received 13 February; accepted 12 August 2011.
Published online 5 October 2011.

1. Doehlemann, G. *et al.* Pep1, a secreted effector protein of *Ustilago maydis*, is required for successful invasion of plant cells. *PLoS Pathog.* **5,** e1000290 (2009).
2. Doehlemann, G. *et al.* Reprogramming a maize plant: transcriptional and metabolic changes induced by the fungal biotroph *Ustilago maydis*. *Plant J.* **56,** 181–195 (2008).
3. Kamper, J. *et al.* Insights from the genome of the biotrophic fungal plant pathogen *Ustilago maydis*. *Nature* **444,** 97–101 (2006).
4. Mueller, O. *et al.* The secretome of the maize pathogen *Ustilago maydis*. *Fungal Genet. Biol.* **45** (suppl. 1), S63–S70 (2008).
5. Bekal, S., Niblack, T. L. & Lambert, K. N. A chorismate mutase from the soybean cyst nematode *Heterodera glycines* shows polymorphisms that correlate with virulence. *Mol. Plant Microbe Interact.* **16,** 439–446 (2003).
6. Doyle, E. A. & Lambert, K. N. *Meloidogyne javanica* chorismate mutase 1 alters plant cell development. *Mol. Plant Microbe Interact.* **16,** 123–131 (2003).
7. Guermeur, Y., Geourjon, C., Gallinari, P. & Deleage, G. Improved performance in protein secondary structure prediction by inhomogeneous score combination. *Bioinformatics* **15,** 413–421 (1999).
8. Sasso, S., Ramakrishnan, C., Gamper, M., Hilvert, D. & Kast, P. Characterization of the secreted chorismate mutase from the pathogen *Mycobacterium tuberculosis*. *FEBS J.* **272,** 375–389 (2005).
9. Eberhard, J., Raesecke, H.-R., Schmid, J. & Amrhein, N. Cloning and expression in yeast of a higher plant chorismate mutase Molecular cloning, sequencing of the cDNA and characterization of the *Arabidopsis thaliana* enzyme expressed in yeast. *FEBS Lett.* **334,** 233–236 (1993).
10. Krappmann, S. *et al.* The *aroC* gene of *Aspergillus nidulans* codes for a monofunctional, allosterically regulated chorismate mutase. *J. Biol. Chem.* **274,** 22275–22282 (1999).
11. Mobley, E. M., Kunkel, B. N. & Keith, B. Identification, characterization and comparative analysis of a novel chorismate mutase gene in *Arabidopsis thaliana*. *Gene* **240,** 115–123 (1999).
12. Basse, C. W., Kolb, S. & Kahmann, R. A maize-specifically expressed gene cluster in *Ustilago maydis*. *Mol. Microbiol.* **43,** 75–93 (2002).
13. Doehlemann, G., Reissmann, S., Assmann, D., Fleckenstein, M. & Kahmann, R. Two linked genes encoding a secreted effector and a membrane protein are essential for *Ustilago maydis*-induced tumour formation. *Mol. Microbiol.* **81,** 751–766 (2011).
14. Skibbe, D. S., Doehlemann, G., Fernandes, J. & Walbot, V. Maize tumors caused by *Ustilago maydis* require organ-specific genes in host and pathogen. *Science* **328,** 89–92 (2010).
15. Bölker, M., Genin, S., Lehmler, C. & Kahmann, R. Genetic regulation of mating and dimorphism in *Ustilago maydis*. *Can. J. Bot.* **73,** 320–325 (1995).
16. Di Stasio, M., Brefort, T., Mendoza-Mendoza, A., Munch, K. & Kahmann, R. The dual specificity phosphatase Rok1 negatively regulates mating and pathogenicity in *Ustilago maydis*. *Mol. Microbiol.* **73,** 73–88 (2009).
17. Wille, A. C., &. Lucas W. J. Ultrastructural and histochemical studies on guard cells. *Planta* **160,** 129–142 (1984).
18. Mobley, E. M., Kunkel, B. N. & Keith, B. Identification, characterization and comparative analysis of a novel chorismate mutase gene in *Arabidopsis thaliana*. *Gene* **240,** 115–123 (1999).
19. Eberhard, J. *et al.* Cytosolic and plastidic chorismate mutase isozymes from *Arabidopsis thaliana*: molecular characterization and enzymatic properties. *Plant J.* **10,** 815–821 (1996).
20. Schnappauf, G., Lipscomb, W. N. & Braus, G. H. Separation of inhibition and activation of the allosteric yeast chorismate mutase. *Proc. Natl Acad. Sci. USA* **95,** 2868–2873 (1998).
21. Schnappauf, G., Strater, N., Lipscomb, W. N. & Braus, G. H. A glutamate residue in the catalytic center of the yeast chorismate mutase restricts enzyme activity to acidic conditions. *Proc. Natl Acad. Sci. USA* **94,** 8491–8496 (1997).
22. Horst, R. J. *et al.* *Ustilago maydis* infection strongly alters organic nitrogen allocation in maize and stimulates productivity of systemic source leaves. *Plant Physiol.* **152,** 293–308 (2010).
23. Glazebrook, J. Contrasting mechanisms of defense against biotrophic and necrotrophic pathogens. *Annu. Rev. Phytopathol.* **43,** 205–227 (2005).

Supplementary Information is linked to the online version of the paper at www.nature.com/nature.

Acknowledgements We are thankful to N. Amrhein and H.-U. Mösch for their comments on the manuscript. We thank B. Valent and C. H. Khang for alerting us to the fact that *Magnaporthe grisea* possesses a secreted chorismate mutase, and are grateful to M. Dickman for allowing us to cite his unpublished results. We thank T. Brefort, E. Mörschel, A. Kaever and M. Landesfeind for experimental support. We acknowledge advice by P. Kast, thank P. Schulze-Lefert for the Gateway-compatible plant transformation vectors, and D. Sicker for providing DIBOA and DIMBOA standards. We acknowledge technical assistance by R. Wissel, S. Löser, D. Vogel, F. Raths, G. Sowa, K. Bolte, M. Johannsen and P. Meyer. Our work was supported through DFG project DJ64/1-1, the collaborative research Center SFB593, and the LOEWE program of the State of Hesse.

Author Contributions A.D., K.S., F.R., V.V., J.K., S.O., T.T., K.F., P.M., Y.-D.S., H.S., A.G. and B.M. designed and performed the wet bench experiments. All authors contributed to data analysis. R.K., A.D. and K.S. wrote the manuscript with input from all co-authors. R.K. directed the project.

Author Information Reprints and permissions information is available at www.nature.com/reprints. The authors declare no competing financial interests. Readers are welcome to comment on the online version of this article at www.nature.com/nature. Correspondence and requests for materials should be addressed to R.K. (kahmann@mpi-marburg.mpg.de).

METHODS

Generation of plasmids. Standard molecular cloning strategies and techniques were applied in this study[24]. Most of the constructs were generated using Gateway technology (Invitrogen) after an insertion of the gene of interest into the pEntry4 vector (Invitrogen) using NcoI and NotI restriction sites. Primers used in this study are described in Supplementary Table 5. Plasmids that were generated in this study are listed in Supplementary Table 6.

Mutant generation and analysis. All *U. maydis* strains (Supplementary Table 7) were generated by gene replacement with PCR-generated constructs or by insertion of p123 derivatives into the *ip* locus as described[25] (Supplementary Table 7). At least three independent mutants were repeatedly tested for virulence on 7-day-old maize seedlings and disease was scored 12 days after infection following described protocols[3]. The widely used solopathogenic haploid strains SG200 and CL13 differ in virulence owing to the presence of autocrine pheromone signalling in SG200 and its absence in CL13, respectively[16]. Compared with the naturally occurring dikaryon, both strains show reduced virulence. Typical symptoms caused by CL13 are depicted in Supplementary Fig. 3a.

Bioinformatic analyses. Signal peptide prediction was performed with the program SignalP 3.0 (http://www.cbs.dtu.dk/services/SignalP/). Chloroplast transit peptides were predicted with the program ChloroP (http://www.cbs.dtu.dk/services/ChloroP/). Sequence alignments were generated using CloneManager Suite 9.0 (www.scied.com). Hierarchical neural network was applied for prediction of the Cmu1 secondary structure at the Network Protein Sequence Analysis server (http://npsa-pbil.ibcp.fr/cgi-bin/npsa_automat.pl?page=npsa_nn.html). Domain analyses were performed with Smart and InterPro (http://smart.embl-heidelberg.de/; http://www.ebi.ac.uk/Tools/InterProScan/).

Quantitative real-time PCR. RNA was extracted from sporidia grown in axenic culture as well as from infected maize plants at the indicated time points with the TRIzol method (Invitrogen), treated with DNase (Ambion) and subsequently used for cDNA synthesis. Quantitative real-time PCR reactions were conducted as described earlier[2]. All reactions were performed at least in biological triplicates. Relative *cmu1* expression levels were calculated in relation to the values obtained for the constitutively expressed peptidyl-prolyl *cis–trans* isomerase gene (*ppi*) of *U. maydis*[26] (Supplementary Table 5).

Yeast complementation assay. Yeast strain Y054679 lacking the *ARO7* gene was transformed with the corresponding pYES and pGad derivatives (Supplementary Table 6) using standard protocols (Clontech) and tested for growth on medium lacking phenylalanine and tryptophan as described previously[19]. A compilation of all *S. cerevisiae* strains used in this study is provided in Supplementary Table 8.

Yeast protein interaction assay. The genes encoding the proteins tested for interaction were cloned into pGBKT7 or pGADT7 vectors (Clontech; Supplementary Table 6), generating in-frame fusions with a gene encoding the yeast *GAL4* binding and activation domain, respectively. Interaction was tested in *S. cerevisiae* AH109 (Clontech). Growth controls were performed on selective dropout media (SD) plates lacking only tryptophan and leucine to select for cells containing the correct plasmids. Protein interactions were assayed on high-stringency SD plates additionally lacking adenine and histidine.

Chorismate mutase activity assays. A glutathione *S*-transferase (GST)–Cmu1$_{22–290}$–HA fusion protein was produced in *Escherichia coli* BL21 containing plasmid pRset-cmu$_{22–290}$–HA (Supplementary Table 6) and enriched by glutathione-affinity purification (GE Healthcare). Also, GST–ZmCm2 fusion protein and derivates of Cmu1 for the enzyme assay were made accordingly. After removal of the GST moiety using PreScission protease (GE Healthcare), chorismate mutase activity assays were performed[27]. After acidic conversion of prephenate to phenylpyruvate the reaction was basidified and extinction at $\lambda = 320$ nm was measured. The increase in extinction was plotted against time (in minutes) to visualize the formation of phenylpyruvate. Error bars represent s.d. from three technical replicates. Purified GST protein was used as a negative control and respective values were subtracted from those obtained with Cmu1$_{22–290}$–HA.

Demonstration of Cmu1 secretion. *U. maydis* strain AB33 P$_{otef}$cmu1–HA was generated by insertion of plasmid p123_otef:um05731–HA into the *ip* locus of AB33[28] (Supplementary Table 7). To analyse Cmu1–HA secretion, material was collected 6 h after induction of filamentous growth in medium containing nitrate[28]. Protein extracts of filamentous cells and culture supernatants (after precipitation with trichloroacetic acid) were subjected to western blot analysis with mouse-anti HA (Sigma) and mouse anti-α-tubulin antibodies (Oncogene).

Biolistic transformation of *Z. mays*. For biolistic transformation[29] of 7- to 10-day-old maize leaves, 1.6-μm gold particles were coated with plasmid DNA coding for the indicated genes driven by the CaMVS35 promoter (Supplementary Table 6). Bombardment was performed using a PDS-1000/He^{TM} instrument (BioRad) at 900 p.s.i. in a 27 Hg vacuum. Fluorescence was observed by confocal microscopy 2 days after transformation.

Confocal and electron microscopy. Confocal microscopy was performed with a LeicaSP5 confocal microscope as described[30]. Wheat germ agglutinin/Alexa Fluor 488 and propidium iodide stains were performed as reported[30]. Autofluorescence was detected at $\lambda = 415–460$ nm.

For immunogold labelling, infected leaf parts were cryofixed by high-pressure freezing (Bal-Tec HPM 010), freeze-substituted in 0.5% glutaraldehyde in acetone (containing 2% H_2O), infiltrated with Lowicryl HM20 and ultraviolet-polymerized at −40 °C. Ultrathin sections were labelled for HA epitope detection using mouse anti-HA (Sigma H9658) and donkey anti-mouse 12-nm gold antibodies (Jackson 715-205-150) and imaged in a Philips CM10 electron microscope at 60 kV.

The distribution of gold particles was determined semi-quantitatively as described[31]. Micrographs of sectioned *Z. mays* samples from infections with SG200 P$_{cmu1}$Cmu1–HA and SG200 P$_{cmu1}$GFP–HA were selected and in each case three different hyphae were chosen. Gold particles on each of the micrographs were then counted and assigned to the plant cell cytosol, the biotrophic interface or the fungal cytosol. The proportional distribution in these compartments was then calculated as a percentage and the s.d. was calculated from the three different data sets for each sample.

Metabolome analyses. For metabolite fingerprinting a section of the third leaf between 1 and 3 cm below the injection holes was excised 8 days after syringe infection with *U. maydis* strains or water (mock control), respectively. For each replicate, 30–40 leaf sections were pooled. Plant material was homogenized under liquid nitrogen. Two or three biological replicates of control leaves and infected leaves (80 mg each) were extracted with methyl-*tert*-butylether/methanol[32]. The polar phase was dried under a nitrogen stream and the extracted metabolites resolved in 10 μl of methanol, 10 μl acetonitrile and 120 μl water. The metabolite analysis was performed by ultra-performance liquid chromatography (UPLC, ACQUITY UPLC System, Waters Corporation) coupled with an orthogonal time-of-flight mass spectrometer (TOF-MS, LCT Premier, Waters Corporation). For LC an ACQUITY UPLC BEH SHIELD RP18 column (1 mm × 100 mm, 1.7 μm particle size, Waters Corporation) was used at a temperature of 40 °C, a flow rate of 0.2 ml min^{-1} and with the following gradient for the analysis of the polar phase: 0–0.5 min 10% B, 0.5–3 min from 10% B to 28% B, 3–8 min from 28% B to 95.5% B, 8–10 min 95.5% B and 10–14 min 10% B (solvent system A: water/formic acid (100:0.1, v/v); B: acetonitrile/formic acid (100:0.1, v/v)). The TOF-MS was operated in negative as well as positive electrospray ionization mode in W optics with a mass resolution larger than 10,000. Data were acquired by MassLynx software (Waters Corporation) in centroided format over a mass range of *m/z* 85–1,200 with scan duration of 0.5 s and an interscan delay of 0.1 s. The capillary and the cone voltage were maintained at 2,700 V and 30 V and the desolvation and source temperature at 350 °C and 80 °C, respectively. Nitrogen was used as cone (30 l h^{-1}) and desolvation gas (800 l h^{-1}). For accurate mass measurement, the TOF-MS was calibrated with phosphoric acid 0.01% (v/v) in acetonitrile/water (50:50, v/v) and the dynamic range enhancement mode was used for data recording. All analyses were monitored by using leucine–enkephaline ($[M + H]^+$ 556.2771 or $[M - H]^-$ 554.2615 as well as its ^{13}C isotopomer $[M + H]^+$ 557.2803 or $[M - H]^-$ 555.2615, Sigma-Aldrich) as lock spray reference compound at a concentration of 0.5 μg ml^{-1} in acetonitrile/water (50:50, v/v) and a flow rate of 30 μl min^{-1}. The raw mass spectrometry data of all samples were processed using the MarkerLynx Application Manager for MassLynx software (Waters Corporation), resulting in two data sets.

The toolbox MarVis (http://marvis.gobics.de33) was used for ranking, filtering, adduct correcting and combining the data as well as for clustering and visualization, respectively. An analysis of variance test was applied to extract a subset of high-quality marker candidates with a p value less than 1×10^{-5}. The filtered data sets were adduct corrected according to the following rules: $[M + H]^+$, $[M + Na]^+$, $[M + NH_4]^+$ for the positive and $[M - H]^-$, $[M + CH_2O_2 - H]^-$, $[M + CH_2O_2 + Na - 2H]^-$ for the negative ionization mode. The combined data led to an overall data set of 810 marker candidates (Supplementary Table 2), which were used for clustering and visualization by means of one-dimensional self-organizing-maps and for database search.

The identity of selected markers was confirmed by MS^2 fragment information[34], co-elution with identical standards or exact mass measurement (Supplementary Table 3).

Salicylic acid measurements. For metabolite fingerprinting, a section of the third leaf between 1 and 3 cm below the injection holes was excised 8 days after syringe infection with *U. maydis* strains or water (mock control), respectively. For each replicate, 30–40 leaf sections were pooled.

Total salicylic acid was extracted[35] and identified by co-elution with an authentic standard using liquid chromatography–mass spectrometry.

Proteome analysis of apoplastic fluids. To extract apoplastic fluids, maize seedlings were infected with a mixture of FB1 and FB2 (ref. 36). Two, four and six days after infection, infected areas were excised and apoplastic fluid was

collected[37]. After precipitation with trichloroacetic acid, proteins were separated by 12% SDS–polyacrylamide gel electrophoresis, digested in gel[38] after subdividing each lane into 11 equal parts and run on an Agilent 1100 nano-HPLC system (75-μm C18 column, 100-min gradients), coupled to an LTQ-FT mass spectrometer (Thermo Scientific). The 'Top-3-SIM' acquisition method was used, as described[39]. Spectra were processed by MSQuant[40] and searched using Mascot against a decoy *Zea*/*Ustilago* protein database. Mass tolerance for the precursor ion was in all cases 5 p.p.m, and for fragment ions 0.5 Da; full trypsin specificity was required and two missed cleavages were allowed. The mean measurement mass deviation of precursor (peptide) ions was 0.96 p.p.m. with a standard deviation of 0.82.

24. Sambrook, J. F. E. & Maniatis, T. *Molecular Cloning: A Laboratory Manual*. Cold Spring Harbor Laboratory Press, 1200 (1989).
25. Loubradou, G., Brachmann, A., Feldbrugge, M. & Kahmann, R. A homologue of the transcriptional repressor Ssn6p antagonizes cAMP signalling in *Ustilago maydis*. *Mol. Microbiol.* **40,** 719–730 (2001).
26. Bohlmann, R. *Isolierung und Charakterisierung von filamentspezifisch exprimierten Genen aus Ustilago maydis.* PhD thesis, Ludwig-Maximilian-Univ. München (1996).
27. Gilchrist, D. G. C. & Conelly, J. A. Chorismate mutase from mung bean and sorghum. *Methods Enzymol.* **142,** 450–463 (1987).
28. Brachmann, A., Weinzierl, G., Kamper, J. & Kahmann, R. Identification of genes in the bW/bE regulatory cascade in *Ustilago maydis*. *Mol. Microbiol.* **42,** 1047–1063 (2001).
29. Ueki, S., Lacroix, B., Krichevsky, A., Lazarowitz, S. G. & Citovsky, V. Functional transient genetic transformation of *Arabidopsis* leaves by biolistic bombardment. *Nature Protocols* **4,** 71–77 (2008).
30. Doehlemann, G. *et al.* Establishment of compatibility in the *Ustilago maydis*/maize pathosystem. *J. Plant Physiol.* **165,** 29–40 (2008).
31. Shimada, Y., Ichinose, S., Sadr, A., Burrow, M. F. & Tagami, J. Localization of matrix metalloproteinases (MMPs-2, 8, 9 and 20) in normal and carious dentine. *Aust. Dent. J.* **54,** 347–354 (2009).
32. Matyash, V., Liebisch, G., Kurzchalia, T. V., Shevchenko, A. & Schwudke, D. Lipid extraction by methyl-tert-butyl ether for high-throughput lipidomics. *J. Lipid Res.* **49,** 1137–1146 (2008).
33. Kaever, A. *et al.* MarVis: a tool for clustering and visualization of metabolic biomarkers. *BMC Bioinformatics* **10,** 92 (2009).
34. Pommerrenig, B. *et al.* Phloem-specific expression of yang cycle genes and identification of novel yang cycle enzymes in plantago and *Arabidopsis*. *Plant Cell* **23,** 1904–1919 (2011).
35. Naranjo, M. A. *et al.* Lithium treatment induces a hypersensitive-like response in tobacco. *Planta* **217,** 417–424 (2003).
36. Banuett, F. & Herskowitz, I. Different a alleles of *Ustilago maydis* are necessary for maintenance of filamentous growth but not for meiosis. *Proc. Natl Acad. Sci. USA* **86,** 5878–5882 (1989).
37. De Wit, P. J. G. M. & Spikman, G. Evidence for the occurence of race and cultivar-specific elicitors of necrosis in intercellular fluids of compatible interactions of *Cladosporium fulvum* and tomato. *Physiol. Plant Pathol.* **21,** 1–11 (1982).
38. Shevchenko, A., Tomas, H., Havlis, J., Olsen, J. V. & Mann, M. In-gel digestion for mass spectrometric characterization of proteins and proteomes. *Nature Protoc.* **1,** 2856–2860 (2006).
39. Olsen, J. V. & Mann, M. Improved peptide identification in proteomics by two consecutive stages of mass spectrometric fragmentation. *Proc Natl Acad Sci USA* **101,** 13417–13422 (2004).
40. Mortensen, P. *et al.* MSQuant, an open source platform for mass spectrometry-based quantitative proteomics. *J. Proteome Res.* **9,** 393–403 (2010).